coatings

MDPI

Article

Optimization of Bulk Heterojunction Organic Photovoltaics

Alaa Y. Ali [1,2,*], Natalie P. Holmes [1,3], Nathan Cooling [1], John Holdsworth [1], Warwick Belcher [1], Paul Dastoor [1] and Xiaojing Zhou [1]

[1] Center of Organic Electronics, University of Newcastle, Newcastle 2308, Australia; natalie.holmes@sydney.edu.au (N.P.H.); nathan.cooling@newcastle.edu.au (N.C.); john.holdsworth@newcastle.edu.au (J.H.); warwick.belcher@newcastle.edu.au (W.B.); paul.dastoor@newcastle.edu.au (P.D.); xiaojing.zhou@newcastle.edu.au (X.Z.)
[2] Department of Physics, College of Education for Pure Science, University of Tikrit, Tikrit 34001, Iraq
[3] Australian Centre for Microscopy and Microanalysis, University of Sydney, Sydney 2006, Australia
* Correspondence: alaa.y.ali@tu.edu.iq

Abstract: The performance of poly(3-hexylthiophene) (P3HT): phenyl-C_{61}-butyric acid methyl ester (PCBM) organic photovoltaic (OPV) devices was found to be strongly influenced by environmental during preparation, thermal annealing conditions, and the material blend composition. We optimized laboratory fabricated devices for these variables. Humidity during the fabrication process can cause electrode oxidation and photo-oxidation in the active layer of the OPV. Thermal annealing of the device structure modifies the morphology of the active layer, resulting in changes in material domain sizes and percolation pathways which can enhance the performance of devices. Thermal annealing of the blended organic materials in the active layer also leads to the growth of crystalline for P3HT domains due to a more arrangement packing of chains in the polymer. Poly(3,4-ethylene dioxythiophene):poly(styrene sulfonate) (PEDOT:PSS) acts as a hole transport layer in these P3HT:PCBM devices. Two commercially materials of PEDOT:PSS were utilizing in the optimization of the OPV in this research; high conductivity PEDOT:PSS-PH1000 and PEDOT:PSS-Al4083, which is specifically designed for OPV interfaces. It was demonstrated that OPVs were prepared with PEDOT:PSS-PH1000 have a less than the average performance of PEDOT:PSS-Al4083. The power conversion efficiency (PCE) decreased clearly with a reducing in masking area devices from 5 mm^2 to 3.8 mm^2 for OPVs based on PH1000 almost absolutely due to the reduced short circuit current (J_{sc}). This work provides a roadmap to understanding P3HT:PCBM OPV performance and outlines the preparation issues which need to be resolved for efficient device fabrication

Keywords: OPV; P3HT:PCBM; PEDOT:PSS; organic heterojunction

Citation: Ali, A.Y.; Holmes, N.P.; Cooling, N.; Holdsworth, J.; Belcher, W.; Dastoor, P.; Zhou, X. Optimization of Bulk Heterojunction Organic Photovoltaics. *Coatings* **2023**, *13*, 1293. https://doi.org/10.3390/coatings13071293

Academic Editor: Ivan Jerman

Received: 12 April 2023
Revised: 8 July 2023
Accepted: 18 July 2023
Published: 24 July 2023

1. Introduction

Over the past two decades, OPV has experienced a considerable increase in interest as a potential energy source due to their semitransparent, flexible, and light-weight properties. In addition to their light harvesting properties, these devices can be fabricated using low-cost manufacturing processes and are suitable for the use of simple laboratory-environment deposition techniques, making research in this area readily accessible [1–4]. However, OPV devices traditionally exhibit lower efficiencies than their silicon counterparts and a significant challenge for the field is how to improve the PCE. In OPV research the most widely studied active layer materials of all of the different possible combinations of organic materials is still P3HT and PCBM due to the low cost and commercial availability of these two components [5]. However, using much more synthetically complex (and therefore expensive) materials, OPV PCEs have now exceeded 18% for OPV devices that included polymer materials as both donors and acceptors [6].

During the lifetime operation of an OPV system, ambient environmental stress such as heat, cold, sunlight, moisture, and mechanical loads can be exposed to and affect the module. These parameters can result in the breakdown of the device structure and a gradual

reduction in the performance of the devices [7]. Consequently, environmental degradation of OPV layers is an important parameter influencing device efficiency. Oxidization and degradation factors for OPVs often are the result of moisture present during laboratory preparation and, thus, water proves a major stress factor for devices. Moisture ingress into devices can result in device layer delamination and cause loss of passivation with degrading of anti-reflection coatings. Furthermore, the corrosion of metal elements in OPV modules appears on devices operated under outdoor conditions [8]. Glen et al. demonstrated the important role humidity contributed to the degradation of OPV devices incorporating Ca/Al and PEDOT:PSS/ITO electrodes, with devices exposed to humid air degrading more rapidly than those in dry air [9]. It has been established that devices incorporating a PEDOT:PSS transport layer are more vulnerable to the influence of moisture due to its hygroscopic nature [10]. Voroshazi et al. demonstrated that moisture leads to significant degradation in OPVs containing a PEDOT:PSS layer by studying OPV devices based on P3HT:PCBM incorporating either MoO_3 or PEDOT:PSS as a hole transport layer [10,11]. Creation of more stable OPV modules can be achieved by avoiding the ingress of moisture [12–14]. Indeed, in order to achieve stable OPV devices, the device must be isolated from water and oxygen in the ambient atmosphere [15]. Even when barrier films are used, oxygen and water diffusion occurs through pinholes in metal electrodes and at the module's edges and boundaries. This ingress leads to modification of the inner surface of the OPV electrodes due to oxidative chemical reactions with them [13,16].

Another key environmental stress parameter for OPV performance is ambient temperature, which can have a significant effect on the electric performance of an OPV system. Generally, the thermal treatment of an OPV increases reaction rates in the component materials, accelerates permeation, and induces mechanical stress on the device relating to dissimilarity of the thermal expansion coefficients of the module parts [17,18]. This treatment can also influence module degradation mechanisms associated with chemical diffusion and reactions. Improved device performance can be obtained through performing various post-fabrication treatments on the OPV module, included the application of thermal annealing [19,20]. However, preventing subsequent changes due to ambient heat or cold is a significant problem. Thermal and solvent vapor annealing is recognized as being of critical importance for optimization of active layer morphology in P3HT:PCBM blends. Annealing processes have been optimized to take advantage of the phase separation of P3HT and PCBM causing the formation of nano-size material domains. These domains are comparable with the length of exciton diffusion in a conjugated polymer [21], maximizing the probability of charge separation. Thermal annealing allows the polymer chains to move into a more crystalline configuration which expels the fullerene directly affecting device properties [22]. In addition, the side chains on the polymer increase device and material stability and affect the solubility of films, allowing for multilayer processing for OPV fabrication [23,24]. Thus, changes to the chemical structure of materials are associated with dramatic differences in morphology and efficiency of devices [25–27].

PEDOT:PSS has often been utilized as a hole transport layer in polymer devices due to its a high optical transparency to visible light [28,29]. Over the last two decades, there have been many studies of different PEDOT:PSS formulations seeking to modify its electronic properties such us work function and electrical conductivity, as well as physical properties (such as wetting properties) [30–32]. Consequently, PEDOT:PSS formulations result in films which exhibit a wide range of conductivities from 10^{-4} to 10^{3} S/cm^{-1}, achieved through synthetic conditions, post-synthesis treatments and doping additives [33]. For PEDOT:PSS, the material work function is high at ~5–5.2 eV which matches well with the highest occupied molecular orbital (HOMO) level of polymer donors in the absorption layer [34]. PEDOT:PSS is almost transparent in the visible light range, exhibiting a transmission of over 90% at 550 nm for a dry film thickness of 100 nm [33]. The π-conjugated structure of the conducting polymer back-bone results in weakly bound electrons [35,36], but the specific conductivity is a result of orbital overlap and delocalization which are limited by the disorder of structure material [36].

PEDOT:PSS (PH1000) is a highly conductive polymer which can be used not only as an hole transport layer but also applied as the transparent electrode in OPV devices due to its excellent flexibility and high transmittance [37–40]. Its highly tunable work function allows excellent alignment of energy levels with active layer polymer blends. The first selected as an inverted conductive polymer in OPV was PEDOT:PSS (Al4083) polymer due to its low temperature process-ability and tunable conductivity [41,42]. Its low work function was shown that limited the value of open-circuit voltage (V_{oc}) in the inverted device [42].

In this report we focus on the impact of fabrication conditions on efficiency s in P3HT:PCBM devices. The discussion outlines the steps which should be considered in the fabrication of P3HT:PCBM OPV to optimize efficiency and prevent degradation.

2. Materials and Methods

Thin layers of PEDOT:PSS (300 nm) was deposited as an aqueous dispersions of low conductivity poly(3,4-ethylene dioxythiophene-poly(styrene sulfonate) (PVP AI4083 (purchased from Heraeus, Hanau, Germany)) and high conductivity of aqueous solution Clevios PH1000 purchased from Heraeus, Hanau, Germany, onto glass substrates, with indium tin oxide (ITO) electrodes, via spin-coated at 4000 rpm for 1 min. The films were dried at 140 °C for 30 min that is removing excess water. The glass/PEDOT:PSS (Al4083 or PH1000) substrates were then directly moved onto a laboratory benchtop under ambient conditions or into a nitrogen (N_2) atmosphere (glovebox) for deposition of the photoactive layer. Both the poly(3-hexylthiophene-2,5-diyl (P3HT)) and (phenyl-C61-butyric acid methyl ester (PCBM) were synthesised inhouse at the University of Newcastle, Callaghan, Australia within the Centre for Organic Electronics [43]. The P3HT:PCBM blends were prepared as a solution via dissolving the materials in 1057 µL of anhydrous 1,2-dichlorobenzene at a concentration ratio of 1:0.8 (20 mg:16 mg total mass) [44]. The solution of polymer-fullerene was sonicated at room temperature for 1 h. For completing dissolution, it was following via stirred overnight. The P3H:PCBM as active layers had spin coating onto substrates of PEDOT:PSS at 900 rpm for 1 min (final thickness ~200 nm) under the two different environmental conditions. The films were dried or pre-annealing (before cathode deposition) under a N2 atmosphere on a hot plate at 60 °C for 4 min for drying and 140 °C for 4 min for pre-annealing. A Calcium (Ca) (~30 nm) was deposited as an interfacial layer onto the active layer by thermal evaporation using Angstrom Engineering evaporator under vacuum (Angstrom Engineering Inc., Cambridge, ON, Canada) to 10–7 bar pressure. This deposition was followed by thermal evaporation of a metal cathode of aluminum (Al) (120 nm under the same condition. Figure 1 illustrates the layered structure of the conventional architecture devices fabricated, which was allowed pathways for charge carriers to be transported towards both the anode and cathode electrodes for collection. The fabricated OPVs were transferred into a N_2 glovebox for the photo-response current density-voltage (J-V) measurement via a Keithley 2400 m. The illumination of OPVs was under an AM1.5 Newport class A solar simulator (Newport Corporation, Irvine, CA, USA) calibrated by a silicon (Si) photodiode.

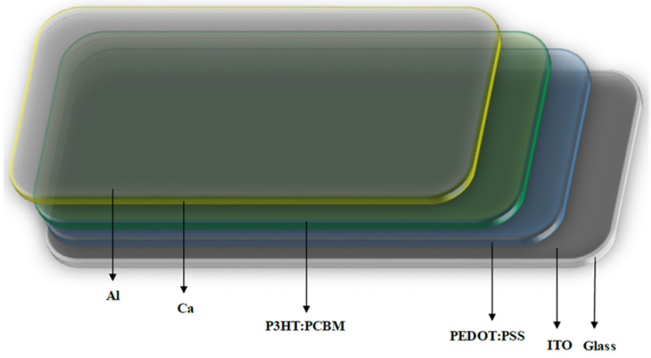

Figure 1. The OPV structure based on an ITO electrode.

3. Results and Discussion

Degradation mechanisms which affect the stability and performance of OPV devices are triggered through different environmental conditions, one of the most critical of which is oxidation of the electrodes by humidity and oxidation in air. In addition, P3HT and PCBM in the active layer is known to be influenced by photo-oxidation under these conditions [45]. The concentration of water and oxygen molecules within the device structure increases in encapsulation OPVs via diffused through barrier and seals film and this increase leads directed to underlie degraded pathway over time [46]. Consequently, OPV stability can be upgraded via removing water and oxygen from the preparation atmosphere. Diffusion of water and oxygen atoms through the OPV layers leads to the formation of corrosion at the electrode interfaces and creates defects in the active layer [47]. In this work, the active layers (P3HT:PCBM) were fabricated under an ambient atmosphere or within a glove box in a clean room under N_2 atmosphere. Table 1 and Figure 2 show the efficiencies of devices prepared under these two conditions and clearly demonstrate the effect of the fabrication environment on the PCE of OPVs, as determined via the current-voltage characteristic. Devices prepared in the wet laboratory are consistently of lower efficiency due to oxidative degradation (2.1% vs. 2.5% average PCE). These results highlight the significant of encapsulated devices in increasing the lifetime and stability of OPV devices.

Table 1. Illustrates OPVs characterization fabricated under two conditions.

Condition	PCE (%)	J_{SC} (mA/cm^2)	V_{OC} (V)	FF	Cell Area (mm^2)
Ambient Atmosphere (Best Device)	2.3	−8.309	0.56	0.49	5
Ambient Atmosphere (Average Data)	2.1	−7.7	0.56	0.5	5
Glove Box (Best Device)	2.88	−9.068	0.57	0.55	5
Glove Box (Average Data)	2.5	−8.2	0.56	0.5	5

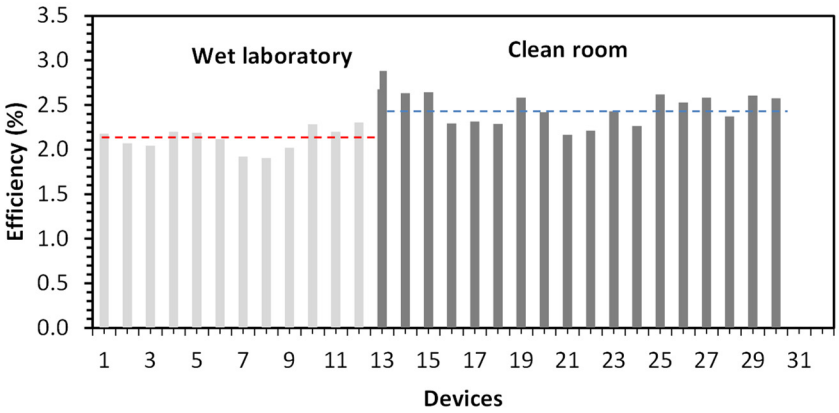

Figure 2. The efficiency of OPVs fabricated under the different atmosphere conditions (Wet laboratory: moist ambient conditions; clean room: under N_2 in a glovebox). The red and blue lines present the average value of efficiency (2.1% and 2.5%).

The preparation of OPV devices through a N_2 atmosphere inside an inert atmosphere glove-box minimizes the undesirable oxidative degradation of the devices. In addition to an overall increase in device efficiency, fill factor (FF) also increases when oxidative degradation is reduced as shown in Figure 3a. The fill factor is largely associated with resistances within the device, particularly at the electrode interfaces, and as such is highly influenced by oxidative degradation of these electrodes [48]. In addition, the exposition of P3HT polymer to oxygen caused a deterioration of polymer properties and damage of its structure [49]. These two factors detrimentally change the shunt and series resistances within the device, lowering FF and thus overall device performance. For devices prepared in the wet laboratory, the humidity could cause a degradation of the P3HT and PEDOT:PSS

and can also lead to a shorter lifetime of the OPV device [47]. Figure 3a shows a higher and more consistent fill factor within the cleanroom synthesized devices comparison to the environment of wet laboratory (0.57 vs. 0.51), highlighting these issues. For the future success of solar energy development of organic devices, these degradation and stability issues must be addressed [45]. The influence of degradation in the active layer was shown for the decreasing values of J_{sc} and V_{oc} in the moist ambient condition as illustrate in Figure 3b,c. There was investigation released that exposure P3HT:PCBM blend to O_2 related to loss value in the dark results of J_{sc} while all factors of OPVs dropped down in the light. It is caused via increasing number of O_2 generated trap states in the polymer active layer [50]. There were many experimental works demonstrating the contributed mechanism of P3HT:PCBM photo-oxide degradation in bulk OPV [51]. The previous study had a clear view that O_2 effected on OPV with gas permeable electrode [52]. Another research work was released that PEDOT:PSS contributed for accelerating oxidation to format that Al oxide in the interface layer between the active layer and Al electrode [53]. It concluded in-contact air to devices in the wet lab (i.e., O_2 atoms reacted to polymer layers). This created different species of oxidized polymer that break polymer chains causing failure in devices performance [54].

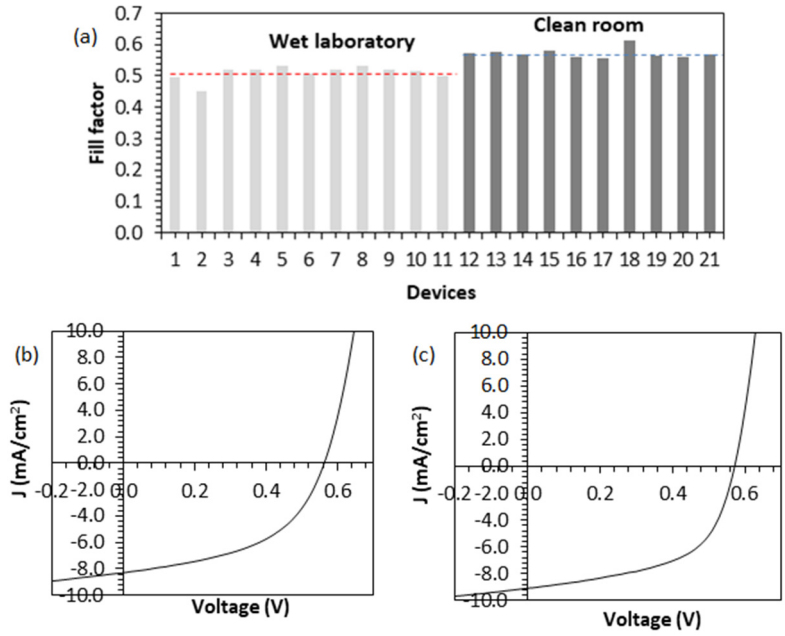

Figure 3. (**a**) the FF of OPV devices fabricated in under the different atmosphere conditions (Wet laboratory: moist ambient conditions, clean room: under N_2 in a glovebox). The FF of OPV devices shows in two atmosphere conditions. The red and blue line are present the average value of FF (0.51 and 0.57), (**b**) J-V curve of OPV fabricated in under moist ambient condition and (**c**) in clean room: under N_2 in a glovebox.

To enhance the device performance, the morphology of active polymer layers was modified by thermal annealing. Thermal annealing has proven to be a remarkable performance-enhancing step when utilizing polymer materials as active layers in OPVs [55]. For example, OPV blends of P3HT:PCBM which are thermal annealed at 80 °C for 5 min have been shown to form crystalline domains of P3HT due to more ordered packing of the polymer chains [56]. In the crystalline domains of P3HT, improved photoconductivity and enhanced hole mobility (which increased from 0.0056 cm^2/Vs for the non-annealed sample to 0.044 cm^2/Vs for the annealed sample) was observed as a result of this morphological change [56]. Thermal annealing is believed to contribute to enhancing the V_{oc}, J_{sc}, and FF in the polymer blend with better charge transport properties for the annealed devices. Comparing to a reference device, the efficiency of OPV devices have improved by up to 3-4-fold

by thermal annealing at 55 °C for 30 min for the P3HT:fullerene system [57]. Overall, the PCE of P3HT:PCBM devices are shown to increase with higher annealing temperatures after the thermal evaporation of OPV electrodes, with PCE improving from 0.4% PCE in a standard device to 2.5% in the annealed device [57]. The improving of the size and modification of domains for donor and acceptor by the thermal annealing also usually leads to enhancements of exciton dissociation, charge separation and charge extraction [55]. For better performance and morphology of P3HT:PCBM devices, optimization of thermal annealing has been significantly influential in the fabrication of efficient OPVs. Studies show that the polymer P3HT changes orientation with the main chain backbones aligning parallel and the side chains orientating themselves perpendicular to the substrate. The PCBM diffusion also forms crystallites of PCBM from the mixed polymer film [58]. In this study we have investigated two annealing conditions prior to electrode deposition; a drying step at 60 °C for 4 min, and an annealing step at 140 °C for 4 min Table 2 and Figure 4 show PCEs for devices treated with both thermal annealing conditions studied. This data clearly shows that annealing at 140 °C for 4 min results in a 60% improvement in PCE, as compared to the 60 °C for 4 min drying conditions. Since the glass transition temperature for P3HT:PCBM increases with PCBM fraction from 12.1 °C for pure P3HT to 131.2 °C for pure PCBM, this result reflects the increased mobility of the blend components, and thus the greater degree of crystallization, present when the film is annealed at the higher temperature [59].

Table 2. Illustrates OPVs characterizations were treated with both thermal annealing conditions.

Condition	PCE (%)	J_{SC} (mA/cm^2)	V_{OC} (V)	FF	Cell Area (mm^2)
Dried Device (Best Device)	1.87	−6.304	0.6	0.49	5
Dried Device (Average Data)	1.6	−5.3	0.59	0.5	5
Annealed Device (Best Device)	2.75	−8.407	0.56	0.57	5

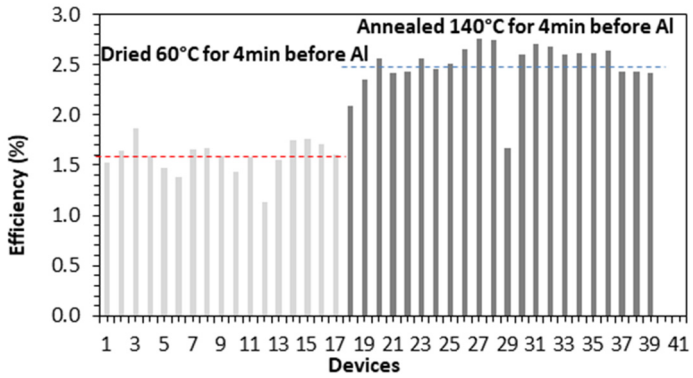

Figure 4. PCEs of P3HT:PCBM OPV devices treated with the dried and thermal annealed conditions. The red and blue line represents the average value of PCE (1.58% and 2.5%, respectively).

Another advantage of thermal annealing is the decreasing of moisture within OPVs, ultimately preventing active layer oxidation, with higher temperatures increasing water evaporation from the polymer structure [60,61]. Generally, P3HT:PCBM device performance is improved by thermal annealing if this step is done either before or after the deposition of Al/Ca electrode [19]. In this study we have annealed the P3HT:PCBM active layer stacks (140 °C for 4 min) both prior to and after deposition of the Al/Ca electrodes. Table 3 and Figure 5 show the PCEs and FF for devices annealed prior to and after electrode deposition. This plot shows clear enhancement of the device which happens when thermal annealing was executed before the deposition of electrode, as comparison to after. In Figure 5a, the PCEs are ~55% higher for OPVs annealed before Al electrode deposition, whilst Figure 5b shows that these same devices exhibited a uniformly higher FF). There

results support the hypothesis that annealing prior to electrode deposition facilitates the release of water from the device, whilst annealing post electrode deposition results in water being trapped within the device architecture, resulting in enhanced oxidative degradation of the device and reduced performance. In accordance with these results, optimal device fabrication conditions for annealing of devices was chosen to be 140 °C for 4 min, prior to electrode deposition.

Table 3. Illustrates OPVs characterizations were annealed prior to and after electrode deposition.

Condition	PCE (%)	J_{SC} (mA/cm^2)	V_{OC} (V)	FF	Cell Area (mm^2)
Annealed before Al (Best Device)	2.75	−8.407	0.56	0.57	5
Annealed before Al (Average Data)	2.5	−7.8	0.56	0.6	5
Annealed after Al (Best Device)	1.85	−6.163	0.59	0.5	5
Annealed after Al (Average Data)	1.6	−5.2	0.6	0.5	5

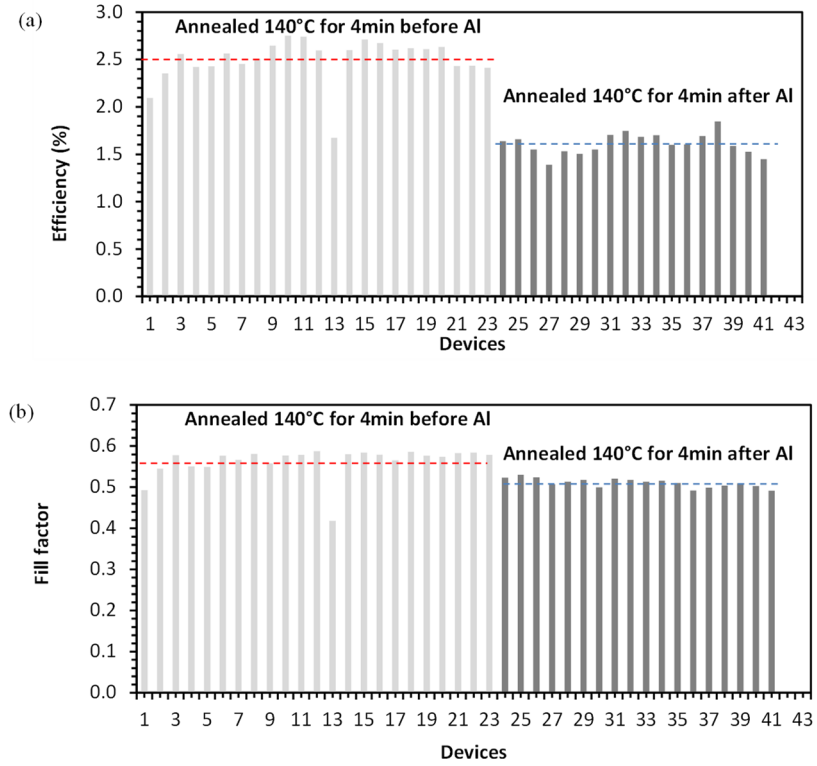

Figure 5. (**a**) PCEs and (**b**) FF of P3HT:PCBM OPVs when thermally annealed before and after the Al/Ca electrodes deposition. The red and blue dashed lines represent the average value of PCE (2.5% and 1.61%) and FF (0.56 and 0.51).

Finally, the importance of the PEDOT:PSS hole transport interlayer was probed by comparing the performance of devices fabricated with a PEDOT:PSS designed for OPV applications (PEDOT:PSS-Al4083) and a high conductivity PEDOT:PSS (Clevios PH100). PEDOT:PSS was applied to the device structure as a solution of polymer electrolyte that contains an excess of positive charge, i.e., the PEDOT is a p-doped material. The location of negative matching charge is in the PSS, which ensures overall the neutral of charge. The PSS also acts as a polymer surfactant which effectively disperses and stabilises the PEDOT in water and other solvents. In large scale printing applications, it has been demonstrated that PEDOT can be a very successful hole-transport layer for OPV [62]. As such, in electrode applications, it was widely utilized as a buffer layer anode in polymer solar cells electrodes [63,64]. The aqueous dispersion of PEDOT:PSS has a high optical transmission in the region of visible light, which is as one of its most desirable polymer OPV

properties. The work function values of PEDOT:PSS have been established to be between 4.8 and 5.2 eV, which allows the formation of an ohmic contact with donor polymers [65], avoiding the formation of energy barriers at the OPV ITO interface. A definite improvement of performance parameters for all P3HT:PCBM conventional solar cells was shown with a PEDOT:PSS as an interlayer at the ITO/active layer interface [66].

Table 4 shows that OPV devices prepared with PEDOT:PSS-PH1000 had a higher average of performance than PEDOT:PSS-Al4083 with an active area of 5 mm^2. Decreasing the masked device area from 5 to 3.8 mm^2 for OPVs based on PH1000 resulted in a marked reduction of the PCE almost exclusively due to J_{SC}. This change in device efficiency is a reflection of the higher conductivity of the PEDOT:PSS, which can allow cross-talk between devices, artificially increasing J_{SC}, and thus device performance, by accessing charges generated outside of the direct illumination area in adjacent devices [67,68]. By comparison OPVs based on Al4083 show more reasonable PCE values when the device size is changed due to the lower conductivity of the interlayer. Moreover, a more stable dark current plot is observed with PEDOT:PSS-Al4083 comparison with the condition of PH1000 (see Figure 6a,b). It is likely that the higher conductivity PEDOT:PSS leads to a leaking current created under dark conditions that is contributing more sheet resistance to the substrate of OPV (see Figure 6b). Another reason for this change could be linked to a worse mismatch of the interface between the interface and OPV active layer [69,70] due to the reduced uniformity of PEDOT:PSS-PH1000. These results demonstrate that Al4083 is the best type of PEDOT:PSS for using in the fabrication of P3HT:PCBM OPVs.

Table 4. Illustrates the characterization of OPVs utilizing two types of PEDOT:PSS in the fabrication.

PEDOT:PSS Type	PCE (%)	J_{SC} (mA/cm^2)	V_{OC} (V)	FF	Cell Area (mm^2)
PEDOT:PSS-PH1000	3.14	−12.36	0.55	0.46	5
PEDOT:PSS-PH1000	2.76	−9.3	0.54	0.55	3.8
PEDOT:PSS-Al 4083	3.06	−8.38	0.55	0.66	5
PEDOT:PSS-Al 4083	3.04	−7.92	0.55	0.7	3.8

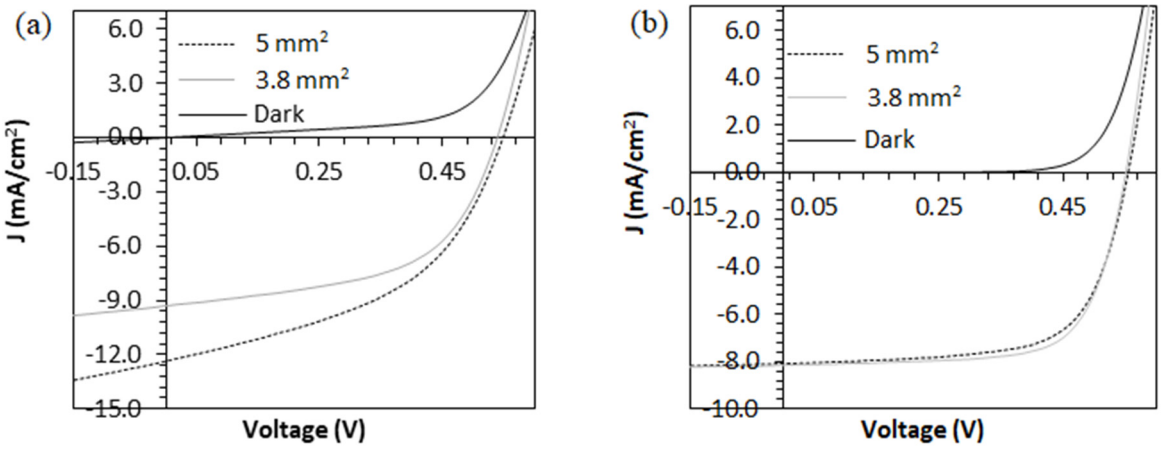

Figure 6. Curves of J-V for OPV devices based on buffer layer of (**a**) PEDOT: PSS-PH1000, and (**b**) PEDOT: PSS-Al 4083.

4. Conclusions

In this article we have highlighted some of the significant challenges of OPV fabrication. Mastering these challenges can raise the performance of devices, particularly with regards to device stability and efficiency. We have shown that it can be possible to improve PCE devices through using one (or more) of these approaches. In particular, controlling environmental conditions during fabrication can dramatically increase the stability of OPV devices. A clear lesion is the importance of capsulation of the device after preparation. The

function of thermal annealing of devices plays an important role in device morphology and performance. The demonstration of increasing values for FF and PCE was achieved by optimizing the thermal annealing of OPVs. Furthermore we have shown that PEDOT:PSS-Al4083 was the most suitable choice as a hole transport interlayer for high performance devices after optimization. These findings should be taken into account to achieve the fabrication of efficient, stable P3HT:PCBM OPV devices.

Author Contributions: Conceptualization and Supervision, X.Z., P.D., W.B. and J.H.; Investigation, A.Y.A.; Writing—original draft preparation, A.Y.A.; Writing—review and editing N.P.H.; Resources N.C. All authors have read and agreed to the published version of the manuscript.

Funding: This research received no external funding.

Institutional Review Board Statement: Not applicable.

Informed Consent Statement: Not applicable.

Data Availability Statement: Not applicable.

Acknowledgments: The financial support for this research was from the Centre for Organic Electronics (COE) at the University of Newcastle, Australia, and we gratefully acknowledge for this support. Alaa Y. Ali also would like to thank the Higher Committee for Education Development in Iraq (HCED-Iraq). This work was performed in part at the Materials node (Newcastle) of the Australian National Fabrication Facility (ANFF), which is a company established under the National Collaborative Research Infrastructure Strategy to provide nano- and microfabrication facilities for Australia's researchers. The researchers would like to thank the Energy Department at the Natural Resources Research Centre and the Department of Physics at the College of Education for Pure Science, Tikrit University, Iraq.

Conflicts of Interest: The authors declare no conflict of interest.

References

1. Günes, S.; Neugebauer, H.; Sariciftci, N.S. Conjugated Polymer-Based Organic Solar Cells. *Chem. Rev.* **2007**, *107*, 1324–1338. [CrossRef]
2. Søndergaard, R.; Hösel, M.; Angmo, D.; Larsen-Olsen, T.T.; Krebs, F.C. Roll-to-roll fabrication of polymer solar cells. *Mater. Today* **2012**, *15*, 36–49. [CrossRef]
3. Liang, Y.; Xu, Z.; Xia, J.; Tsai, S.-T.; Wu, Y.; Li, G.; Ray, C.; Yu, L. For the Bright Future—Bulk Heterojunction Polymer Solar Cells with Power Conversion Efficiency of 7.4%. *Adv. Mater.* **2010**, *22*, E135–E138. [CrossRef]
4. Huang, H.-L.; Lee, C.-T.; Lee, H.-Y. Performance improvement mechanisms of P3HT:PCBM inverted polymer solar cells using extra PCBM and extra P3HT interfacial layers. *Org. Electron.* **2015**, *21*, 126–131. [CrossRef]
5. Green, M.A.; Emery, K.; Hishikawa, Y.; Warta, W.; Dunlop, E.D. NIMS sets a new world record for the highest conversion efficiency in dye-sensitized solar cells. *Prog. Photovolt.* **2012**, *20*, 12–20. [CrossRef]
6. Wang, J.; Cui, Y.; Xu, Y.; Xian, K.; Bi, P.; Chen, Z.; Zhou, K.; Ma, L.; Zhang, T.; Yang, Y.; et al. A New Polymer Donor Enables Binary All-Polymer Organic Photovoltaic Cells with 18% Efficiency and Excellent Mechanical Robustness. *Adv. Mater.* **2022**, *34*, 2205009. [CrossRef] [PubMed]
7. SolarPower Europe; ETIP PV. *Solar Skins: An Opportunity for Greener Cities*; SolarPower Europe; ETIP PV: Brussels, Belgium, 2019.
8. Soares, G.A.; David, T.W.; Anizelli, H.; Miranda, B.; Rodrigues, J.; Lopes, P.; Martins, J.; Cunha, T.; Vilaça, R.; Kettle, J.; et al. Outdoor performance of organic photovoltaics at two different locations: A comparison of degradation and the effect of condensation. *J. Renew. Sustain. Energy* **2020**, *12*, 063502. [CrossRef]
9. Glen, T.; Scarratt, N.; Yi, H.; Iraqi, A.; Wang, T.; Kingsley, J.; Buckley, A.; Lidzey, D.; Donald, A. Grain size dependence of degradation of aluminium/calcium cathodes in organic solar cells following exposure to humid air. *Sol. Energy Mater. Sol. Cells* **2015**, *140*, 25–32. [CrossRef]
10. Voroshazi, E.; Verreet, B.; Buri, A.; Müller, R.; Di Nuzzo, D.; Heremans, P. Influence of cathode oxidation via the hole extraction layer in polymer: Fullerene solar cells. *Org. Electron.* **2011**, *12*, 736–744. [CrossRef]
11. Sun, Y.; Takacs, C.J.; Cowan, S.R.; Seo, J.H.; Gong, X.; Roy, A.; Heeger, A.J. Efficient, air-stable bulk heterojunction polymer solar cells using MoOx as the anode interfacial layer. *Adv. Mater.* **2011**, *23*, 2226–2230. [CrossRef]
12. Norrman, K.; Alstrup, J.; Jørgensen, M.; Krebs, F.C. Lifetimes of organic photovoltaics: Photooxidative degradation of a model compound. *Surf. Interface Anal.* **2006**, *38*, 1302–1310. [CrossRef]
13. Norrman, K.; Gevorgyan, S.A.; Krebs, F.C. Water-Induced Degradation of Polymer Solar Cells Studied by H218O Labeling. *ACS Appl. Mater. Interfaces* **2009**, *1*, 102–112. [CrossRef] [PubMed]

14. Burrows, P.E.; Graff, G.L.; Gross, M.E.; Martin, P.M.; Hall, M.; Mast, E.; Bonham, C.C.; Bennett, W.D.; Michalski, L.A.; Weaver, M.S.; et al. Gas permeation and lifetime tests on polymer-based barrier coatings. In *Organic Light-Emitting Materials and Devices IV*; SPIE: Bellingham, WA, USA, 2001; Volume 4105.
15. Cros, S.; de Bettignies, R.; Berson, S.; Bailly, S.; Maisse, P.; Lemaitre, N.; Guillerez, S. Definition of encapsulation barrier requirements: A method applied to organic solar cells. *Sol. Energy Mater. Sol. Cells* **2011**, *95*, S65–S69. [CrossRef]
16. Nyga, A.; Blacha-Grzechnik, A.; Podsiadły, P.; Duda, A.; Kępska, K.; Krzywiecki, M.; Motyka, R.; Janssen, R.A.J.; Data, P. Singlet oxygen formation from photoexcited P3HT: PCBM films applied in oxidation reactions. *Mater. Adv.* **2022**, *3*, 2063–2069. [CrossRef]
17. Kettle, J.; Stoichkov, V.; Kumar, D.; Corazza, M.; Gevorgyan, S.; Krebs, F.C. Using ISOS consensus test protocols for development of quantitative life test models in ageing of organic solar cells. *Sol. Energy Mater. Sol. Cells* **2017**, *167*, 53–59. [CrossRef]
18. Arrhenius, S. Über die Dissociationswärme und den Einfluss der Temperatur auf den Dissociationsgrad der Elektrolyte. *Z. Für Phys. Chem.* **1889**, *4U*, 96–116. [CrossRef]
19. Ma, W.; Yang, C.; Gong, X.; Lee, K.; Heeger, J. Thermally Stable, Efficient Polymer Solar Cells with Nanoscale Control of the Interpenetrating Network Morphology. *Adv. Funct. Mater.* **2005**, *15*, 1617–1622. [CrossRef]
20. Mihailetchi, V.D.; Xie, H.X.; de Boer, B.; Koster, L.J.A.; Blom, P.W.M. Charge Transport and Photocurrent Generation in Poly(3-hexylthiophene): Methanofullerene Bulk-Heterojunction Solar Cells. *Adv. Funct. Mater.* **2006**, *16*, 699–708. [CrossRef]
21. De Luca, G.; Treossi, E.; Liscio, A.; Mativetsky, J.M.; Scolaro, L.M.; Palermo, V.; Samorì, P. Solvent vapour annealing of organic thin films: Controlling the self-assembly of functional systems across multiple length scales. *J. Mater. Chem.* **2010**, *20*, 2493–2498. [CrossRef]
22. Verploegen, E.; Mondal, R.; Bettinger, C.J.; Sok, S.; Toney, M.F.; Bao, Z. Effects of Thermal Annealing Upon the Morphology of Polymer–Fullerene Blends. *Adv. Funct. Mater.* **2010**, *20*, 3519–3529. [CrossRef]
23. Manceau, M.; Helgesen, M.; Krebs, F.C. Thermo-cleavable polymers: Materials with enhanced photochemical stability. *Polym. Degrad. Stab.* **2010**, *95*, 2666–2669. [CrossRef]
24. Kuhn, M.; Ludwig, J.; Marszalek, T.; Adermann, T.; Pisula, W.; Müllen, K.; Colsmann, A.; Hamburger, M. Tertiary Carbonate Side Chains: Easily Tunable Thermo-labile Breaking Points for Controlling the Solubility of Conjugated Polymers. *Chem. Mater.* **2015**, *27*, 2678–2686. [CrossRef]
25. Gao, K.; Deng, W.; Xiao, L.; Hu, Q.; Kan, Y.; Chen, X.; Wang, C.; Huang, F.; Peng, J.; Wu, H.; et al. New insight of molecular interaction, crystallization and phase separation in higher performance small molecular solar cells via solvent vapor annealing. *Nano Energy* **2016**, *30*, 639–648. [CrossRef]
26. Li, Z.; Jiang, K.; Yang, G.; Lai, J.Y.L.; Ma, T.; Zhao, J.; Ma, W.; Yan, H. Donor polymer design enables efficient non-fullerene organic solar cells. *Nat. Commun.* **2016**, *7*, 13094. [CrossRef] [PubMed]
27. Liu, Y.; Zhao, J.; Li, Z.; Mu, C.; Ma, W.; Hu, H.; Jiang, K.; Lin, H.; Ade, H.; Yan, H. Aggregation and morphology control enables multiple cases of high-efficiency polymer solar cells. *Nat. Commun.* **2014**, *5*, 5293. [CrossRef] [PubMed]
28. Lee, Y.J.; Yeon, C.; Lim, J.W.; Yun, S.J. Flexible p-type PEDOT: PSS/a-Si: H hybrid thin film solar cells with boron-doped interlayer. *Sol. Energy* **2018**, *163*, 398–404. [CrossRef]
29. Benten, H.; Mori, D.; Ohkita, H.; Ito, S. Recent research progress of polymer donor/polymer acceptor blend solar cells. *J. Mater. Chem. A* **2016**, *4*, 5340–5365. [CrossRef]
30. Kim, Y.H.; Sachse, C.; Machala, M.L.; May, C.; Müller-Meskamp, L.; Leo, K. Highly Conductive PEDOT:PSS Electrode with Optimized Solvent and Thermal Post-Treatment for ITO-Free Organic Solar Cells. *Adv. Funct. Mater.* **2011**, *21*, 1076–1081. [CrossRef]
31. Yan, H.; Okuzaki, H. Effect of solvent on PEDOT/PSS nanometer-scaled thin films: XPS and STEM/AFM studies. *Synth. Met.* **2009**, *159*, 2225–2228. [CrossRef]
32. Tait, J.G.; Worfolk, B.J.; Maloney, S.A.; Hauger, T.C.; Elias, A.L.; Buriak, J.M.; Harris, K.D. Spray coated high-conductivity PEDOT:PSS transparent electrodes for stretchable and mechanically-robust organic solar cells. *Sol. Energy Mater. Sol. Cells* **2013**, *110*, 98–106. [CrossRef]
33. Sun, K.; Zhang, S.; Li, P.; Xia, Y.; Zhang, X.; Du, D.; Isikgor, F.H.; Ouyang, J. Review on application of PEDOTs and PEDOT: PSS in energy conversion and storage devices. *J. Mater. Sci. Mater. Electron.* **2015**, *26*, 4438–4462. [CrossRef]
34. Zhang, F.; Johansson, M.; Andersson, M.R.; Hummelen, J.C.; Inganäs, O. Polymer photovoltaic cells with conducting polymer anodes. *Adv. Mater.* **2002**, *14*, 662–665. [CrossRef]
35. Berggren, M.; Malliaras, G.G. How conducting polymer electrodes operate. *Science* **2019**, *364*, 233–234. [CrossRef] [PubMed]
36. Paulsen, B.D.; Tybrandt, K.; Stavrinidou, E.; Rivnay, J. Organic mixed ionic–electronic conductors. *Nat. Mater.* **2020**, *19*, 13–26. [CrossRef] [PubMed]
37. Xu, Y.; Lin, Z.; Wei, W.; Hao, Y.; Liu, S.; Ouyang, J.; Chang, J. Recent progress of electrode materials for flexible perovskite solar cells. *Nano-Micro Lett.* **2022**, *14*, 117. [CrossRef]
38. Sun, K.; Li, P.; Xia, Y.; Chang, J.; Ouyang, J. Transparent conductive oxide-free perovskite solar cells with PEDOT: PSS as transparent electrode. *ACS Appl. Mater. Interfaces* **2015**, *7*, 15314–15320. [CrossRef] [PubMed]
39. Lee, G.; Kim, M.-C.; Choi, Y.W.; Ahn, N.; Jang, J.; Yoon, J.; Kim, S.M.; Lee, J.-G.; Kang, D.; Jung, H.S.; et al. Ultra-flexible perovskite solar cells with crumpling durability: Toward a wearable power source. *Energy Environ. Sci.* **2019**, *12*, 3182. [CrossRef]
40. Xie, H.; Liang, T.; Yin, X.; Liu, J.; Liu, D.; Wang, G.; Gao, B.; Que, W. Mechanical Stability Study on PEDOT: PSS-Based ITO-Free Flexible Perovskite Solar Cells. *ACS Appl. Energy Mater.* **2022**, *5*, 3081–3091. [CrossRef]

41. You, J.; Hong, Z.; Yang, Y.; Chen, Q.; Cai, M.; Song, T.-B.; Chen, C.-C.; Lu, S.; Liu, Y.; Zhou, H. Low-temperature solution-processed perovskite solar cells with high efficiency and flexibility. *ACS Nano* **2014**, *8*, 1674–1680. [CrossRef]
42. Yang, Z.; Chueh, C.-C.; Zuo, F.; Kim, J.H.; Liang, P.-W.; Jen, A.K.-Y. High-performance fully printable perovskite solar cells via blade-coating technique under the ambient condition. *Adv. Energy Mater.* **2015**, *5*, 1500328. [CrossRef]
43. Cooling, N.A.; Barnes, E.F.; Almyahi, F.; Feron, K.; Al-Mudhaffer, M.F.; Al-Ahmad, A.; Vaughan, B.; Andersen, T.R.; Griffith, M.J.; Hart, A.S.; et al. A low-cost mixed fullerene acceptor blend for printed electronics. *J. Mater. Chem. A* **2016**, *4*, 10274–10281. [CrossRef]
44. Ali, A.Y.; Holmes, N.P.; Ameri, M.; Feron, K.; Thameel, M.N.; Barr, M.G.; Fahy, A.; Holdsworth, J.; Belcher, W.; Dastoor, P.; et al. Low-Temperature CVD-Grown Graphene Thin Films as Transparent Electrode for Organic Photovoltaics. *Coatings* **2022**, *12*, 681. [CrossRef]
45. Seemann, A.; Sauermann, T.; Lungenschmied, C.; Armbruster, O.; Bauer, S.; Egelhaaf, H.J.; Hauch, J. Reversible and irreversible degradation of organic solar cell performance by oxygen. *Sol. Energy* **2011**, *85*, 1238–1249. [CrossRef]
46. Norrman, K.; Krebs, F.C. Lifetimes of organic photovoltaics: Using TOF-SIMS and $^{18}O_2$ isotopic labelling to characterise chemical degradation mechanisms. *Sol. Energy Mater. Sol. Cells* **2006**, *90*, 213–227. [CrossRef]
47. Madogni, V.I.; Kounouhéwa, K.; Akpo, A.; Agbomahéna, M.; Hounkpatin, S.A.; Awanou, C.N. Comparison of degradation mechanisms in organic photovoltaic devices upon exposure to a temperate and a subequatorial climate. *Chem. Phys. Lett.* **2015**, *640*, 201–214. [CrossRef]
48. Qi, B.; Wang, J. Fill factor in organic solar cells. *Phys. Chem. Chem. Phys.* **2013**, *15*, 8972–8982.
49. Grossiord, N.; Kroon, J.M.; Andriessen, R.; Blom, P.W. Degradation mechanisms in organic photovoltaic devices. *Org. Electron.* **2012**, *13*, 432–456. [CrossRef]
50. Schafferhans, J.; Baumann, A.; Wagenpfahl, A.; Deibel, C.; Dyakonov, V. Oxygen doping of P3HT:PCBM blends: Influence on trap states, charge carrier mobility and solar cell performance. *Org. Electron.* **2010**, *11*, 1693–1700. [CrossRef]
51. Yang, W.; Yao, Y.; Wu, C.-Q. Mechanisms of device degradation in organic solar cells: Influence of charge injection at the metal/organic contacts. *Org. Electron.* **2013**, *14*, 1992–2000. [CrossRef]
52. Ameri, T.; Dennier, G.; Waldauf, C.; Azimi, H.; Seemann, A.; Forberich, K.; Hauch, J.; Hingeril, K.; Brabec, C.J. Fabrication, Optical Modeling, and Color Characterization of Semitransparent Bulk-Heterojunction Organic Solar Cells in an Inverted Structure. *Adv. Funct. Mater.* **2010**, *20*, 1592–1598. [CrossRef]
53. Yamanari, T.; Taima, T.; Sakai, J.; Tsukamoto, J.; Yoshida, Y. Effect of buffer layers on stability of polymer-based organic solar cells. *Jpn. J. Appl. Phys.* **2010**, *49*, 01AC02. [CrossRef]
54. Chambon, S.; Rivaton, A.; Gardette, J.L.; Firon, M.; Lutsen, L.; Polym, J. Aging of a donor conjugated polymer: Photochemical studies of the degradation of poly[2-methoxy-5-(3′,7′-dimethyloctyloxy)-1,4-phenylenevinylene]. *J. Polym. Sci. Part A Polym. Chem.* **2007**, *45*, 317–331. [CrossRef]
55. Wang, T.; Pearson, A.J.; Lidzey, D.G.; Jones, R.A.L. Evolution of Structure, Optoelectronic Properties, and Device Performance of Polythiophene: Fullerene Solar Cells During Thermal Annealing. *Adv. Funct. Mater.* **2011**, *21*, 1383–1390. [CrossRef]
56. Savenije, T.J.; Kroeze, J.E.; Yang, X.; Loos, J. The Effect of Thermal Treatment on the Morphology and Charge Carrier Dynamics in a Polythiophene–Fullerene Bulk Heterojunction. *Adv. Funct. Mater.* **2005**, *15*, 1260–1266. [CrossRef]
57. Padinger, F.; Rittberger, R.; Sariciftci, N. Effects of Postproduction Treatment on Plastic Solar Cells. *Adv. Funct. Mater.* **2003**, *13*, 85–88. [CrossRef]
58. Erb, T.; Zhokhavets, U.; Gobsch, G.; Raleva, S.; Stühn, B.; Schilinsky, P.; Waldauf, C.; Brabec, C.J. Correlation Between Structural and Optical Properties of Composite Polymer/Fullerene Films for Organic Solar Cells. *Adv. Funct. Mater.* **2005**, *15*, 1193–1196. [CrossRef]
59. Zhao, J.; Swinnen, Z.; Van Assche, G.; Manca, J.; Vanderzande, D.; Van Mele, B. Phase Diagram of P3HT/PCBM Blends and Its Implication for the Stability of Morphology. *J. Phys. Chem. B* **2009**, *113*, 1587–1591. [CrossRef] [PubMed]
60. Bouaziz, J.; Cancellieri, C.; Rheingans, B.; Jeurgens, L.P.H.; La Mattina, F. Advanced Epitaxial Lift-Off and Transfer Procedure for the Fabrication of High-Quality Functional Oxide Membranes. *Adv. Mater. Interfaces* **2023**, *10*, 2201458. [CrossRef]
61. Rui, Y.; Jin, Z.; Fan, X.; Li, W.; Li, B.; Li, T.; Wang, Y.; Wang, L.; Liang, J. Defect passivation and electrical conductivity enhancement in perovskite solar cells using functionalized graphene quantum dots. *Mater. Futures* **2022**, *1*, 045101. [CrossRef]
62. Po, R.; Carbonera, C.; Bernardi, A.; Tinti, F.; Camaioni, N. Polymer- and carbon-based electrodes for polymer solar cells: Toward low-cost, continuous fabrication over large area. *Sol. Energy Mater. Sol. Cells* **2012**, *100*, 97–114. [CrossRef]
63. Po, R.; Chiara, C.; Bernardi, A.; Camaioni, N. The role of buffer layers in polymer solar cells. *Energy Environ. Sci.* **2011**, *4*, 285–310. [CrossRef]
64. Irwin, M.D.; Buchholz, D.B.; Hains, A.W.; Chang, R.P.H.; Marks, T.J. *p*-Type semiconducting nickel oxide as an efficiency-enhancing anode interfacial layer in polymer bulk-heterojunction solar cells. *Proc. Natl. Acad. Sci. USA* **2008**, *105*, 2783–2787.
65. Brabec, C.; Scherf, U.; Dyakonov, V. (Eds.) *Organic Photovoltaics: Materials, Device Physics, and Manufacturing Technologies*; Wiley-VCH Verlag GmbH & Co. KGaA: Weinheim, Germany, 2008; Chapter 7.
66. Li, G.; Chu, C.-W.; Shrotriya, V.; Huang, J.; Yang, Y. Efficient inverted polymer solar cells. *Appl. Phys. Lett.* **2006**, *88*, 253503. [CrossRef]
67. Su, Y.-W.; Lan, C.-S.; Wei, K.-H. Organic photovoltaics. *Mater. Today* **2012**, *15*, 554–562. [CrossRef]

68. Kiermasch, D.; Gil-Escrig, L.; Bolink, H.J.; Tvingstedt, K. Effects of Masking on Open-Circuit Voltage and Fill Factor in Solar Cells. *Joule* **2019**, *3*, 16–26.
69. Wang, G.; Ma, L.-J.; Lei, B.-X.; Wu, H.; Liu, Z.-Q. Enhanced electron transport through two-dimensional Ti3C2 in dye-sensitized solar cells. *Rare Met.* **2022**, *41*, 3078–3085.
70. Su, Y.-W.; Huang, Y.-S.; Huang, H.-C.; Chen, P.-T. Optoelectronic Properties of a Benzodithiophene-Based Organic Photovoltaic. *ECS J. Solid State Sci. Technol.* **2021**, *10*, 075003. [CrossRef]